(ALCL and ALK-positive large B-cell lymphoma[28]) and sarcoma (IMT,[5] rhabdomyosarcoma,[26] and neuroblastoma[29]). It was not until 2007 that the presence of an ALK fusion was described in lung cancer.[6] This seems to be mainly because EML4-ALK is barely detectable by conventional anti-ALK immunohistochemistry. Considering in reverse, in cases of a tumor that is positive by anti-ALK iAEP immunohistochemistry, but negative by conventional anti-ALK immunohistochemistry, the tumor may have a novel ALK fusion partner, or express wild-type ALK at a modest level. Indeed, in "ALK-negative" IMT cases defined by conventional ALK immunohistochemistry, PPFIBP1-ALK was identified through reassessment for ALK fusions, using anti-ALK iAEP immunohistochemistry.[24] This prompted us to reevaluate other types of solid cancers for ALK fusions. Here, we describe the identification of TPM3-ALK (fusion of tropomyosin 3 and ALK) and EML4-ALK in renal cancer, by anti-ALK iAEP immunohistochemistry.

MATERIALS AND METHODS

Materials

We examined 355 renal tumor tissues from patients who had received surgery in the Cancer Institute Hospital, Japanese Foundation for Cancer Research, Tokyo, between 1994 and 2010. Renal tumors included 255 clear cell renal cell carcinomas (RCCs), 32 papillary RCCs, 34 chromophobe RCCs, 6 collecting duct carcinomas, 10 unclassified RCCs, 6 sarcomatoid RCCs, and 12 other tumors (4 oncocytomas, 3 angiomyolipomas, 1 solitary fibrous tumor, 2 spindle cell sarcomas, 1 desmoplastic sarcoma, and 1 anaplastic carcinoma). Surgically removed tumor specimens were routinely fixed in 20% neutralized formalin and embedded in paraffin for conventional histopathological examination. Immunohistochemical screenings were performed using tissue microarrays. For the 2 cases positive for anti-ALK immunohistochemistry, total RNA was extracted from the corresponding snap-frozen specimen, and purified with the use of an RNeasy Mini kit (Qiagen, Tokyo, Japan). Informed consent was obtained from the patients. The study was approved by the institutional review board of the Japanese Foundation for Cancer Research.

Immunohistochemistry

Formalin-fixed, paraffin-embedded tissue was sliced at a thickness of 4 μm, and the sections were placed on silane-coated slides. For antigen retrieval, the slides were heated for 45 minutes at 102°C in antigen retrieval solution (Nichirei Bioscience, Tokyo). For conventional immunostaining, the slides were incubated at room temperature with primary antibodies: ALK (5A4), vimentin, epithelial membrane antigen (EMA), cytokeratin 7, AE1/AE3, CAM5.2, 34βE12, α-methylacyl-coenzymeA racemase (AMACR), clusters of differentiation 10 (CD10), transcription termination factor 1 (TTF1), renal cell carcinoma marker (RCC Ma), paired box 2 (PAX2), and paired box 8 (PAX8) for 30 minutes. The immune complexes were then detected with polymer reagent (Histofine Simple Stain MAX PO; Nichirei Bioscience, Tokyo, Japan). For the sensitive detection of ALK fusion proteins, the ALK Detection Kit (Nichirei Bioscience), which is based on the iAEP method, was used.

Isolation of ALK Fusions

To obtain complementary DNA (cDNA) fragments corresponding to a novel ALK fusion gene, we used a 5′ rapid amplification of cDNA ends (5′-RACE) method with the SMARTer RACE cDNA Amplification Kit (Clontech, Takara Bio Inc., Shiga, Japan). We followed the manufacturer's instructions, with a minor modification: the ALK2458R primer (5′-GTAGTTGGGGTTGTAGTC GGTCATGATGGT-3′) was used as the gene-specific reverse primer. From the deoxythymidine oligomer–primed cDNA obtained from RNA from case 1, a 385–base pair (bp) cDNA fragment containing the fusion point was specifically amplified with the primers TPM3-705F (5′-AGAGACCCGTGCTGAGTTTGCTG-3′) and ALK3078RR (5′-ATCCAGTTCGTCCTGTTCA GAGC-3′). From case 2, a 454-bp cDNA fragment containing the fusion point was specifically amplified with the primers EML4-72F (5′-GTCAGCTCTTGAGT CACGAGTT-3′) and ALK3078RR. Polymerase chain reaction (PCR) analysis of genomic DNA for TPM3-ALK in case 1 was carried out with a pair of primers flanking the putative fusion point: TPM3-705F (5′-AGA GACCCGTGCTGAGTTTGCTG-3′) and Fusion-RT-AS (5′-TCTTGCCAGCAAAGCAGTAGTTGG-3′). For genomic PCR analysis of EML4-ALK in case 2, we used primers EML4-107F (5′-ATGAAATCACTGTGCTAA AGGCGGCT-3′) and Fusion-RT-AS (5′-TCTTGCCA GCAAAGCAGTAGTTGG-3′).

Fluorescence In Situ Hybridization

Fluorescence in situ hybridization (FISH) analysis of gene fusion was carried out with DNA probes for ALK, TPM3, EML4, and transcription factor E3 (TFE3). Unstained sections (4 μm thick) were subjected to hybridization with an ALK-split probe set (Dako, Tokyo, Japan), TFE3-split probe set (Kreatech, Amsterdam, The Netherlands), or bacterial artificial chromosome (BAC) clone-derived

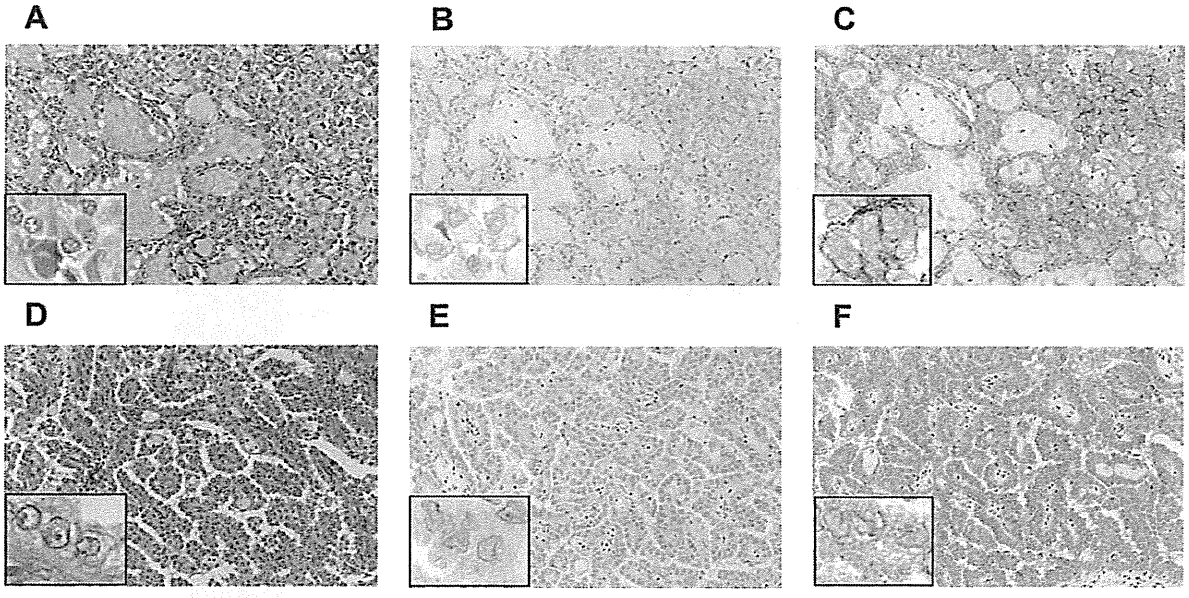

Figure 2. Histopathology of anaplastic lymphoma kinase (ALK)-positive renal cancer. Cuboidal tumor cells showed papillary, tubular, or cribriform growth patterns. The tumor cells had eosinophilic cytoplasm and round to ovoid nuclei. (A) The glandular structures possessed abundant mucin. (D) The tumor comprised a papillary structure of cuboidal or low columnar cells, with eosinophilic cytoplasm and small uniform round to oval nuclei (A,D hematoxylin and eosin stain). The tumor cells were (B) weakly positive and (E) indeterminate for ALK with conventional anti-ALK immunohistochemistry. (C,F) All of the tumor cells were clearly positive for ALK when the iAEP method was used. The staining pattern was diffuse cytoplasmic, with (C) membranous or (F) fine granular accentuation. Figures were taken using the corresponding whole sections (× 10 objective for low power view. × 40 objective for inset). Case 1 (A-C); Case 2 (D-F).

probes for ALK (RP11-984I21, RP11-62B19, RP11-701P18), TPM3 (RP11-809B24), and EML4 (RP11-996L7). Hybridized slides were then stained with 4′,6-diamidino-2-phenylindole and examined using a fluorescence microscope BX51 (Olympus, Tokyo, Japan).

Mutation Analyses for MET

A 1007-bp cDNA fragment containing the MET kinase domain was amplified using the primers MET-3186F (5′-GTCCATTACTGCAAAATACTGTCC-3′) and MET-4193R (5′-CACCTCATCATCAGCGTTATC-3′). The PCR product was sequenced after subcloning.

RESULTS

Identification of ALK Fusions in RCC Samples

Sections of tissue microarray were immunostained for ALK by the iAEP method, resulting in the detection of 2 positive cases (case 1, Fig. 2A-C; case 2, Fig. 2D-F). The positive results were also confirmed using corresponding whole histopathological sections, in which all of the tumor cells stained for ALK as other ALK-positive cancers usually do. We carried out 5′-RACE assays to determine whether these cases expressed ALK fusion or full-length ALK (mutated or unmutated). We isolated a cDNA fragment containing the exon 8 of *TPM3* fused in-frame to the exon 20 of *ALK* (Fig. 3A) in case 1, and the exon 2 of *EML4* fused to the exon 20 of *ALK* in case 2 (Fig. 3B). This EML4-ALK is called variant 5 (E2;A20) in lung cancer.[30] Reverse transcription PCR (RT-PCR) assays designed for the *TPM3-ALK* or E2;A20 successfully amplified cDNAs containing the fusion points (Fig. 3C,D). To confirm the genomic rearrangement, we performed FISH assays (Fig. 4) and genomic PCR (data not shown) for each fusion. All our results were consistent with the presence of t(1;2)(p21;p23)/*TPM3-ALK* in case 1, or inv(2)(p21p23)/E2;A20 in case 2. No other cases were positive for ALK by iAEP immunohistochemistry. All 355 cases were further examined by ALK-split FISH assay. In 12 of the cases, FISH was unsuccessful and not evaluable. In the other cases, the results were identical to those obtained by anti-ALK iAEP immunohistochemistry.

Case Presentation

Case 1

The patient was a 36-year-old woman who had a complaint suggestive of pyelonephritis. Magnetic resonance imaging and computed tomography showed a mass (4.0 cm × 4.0 cm × 3.5 cm) in the left kidney. No metastatic lesions or lymph node enlargements were identified. The patient had no past medical history of malignancy.

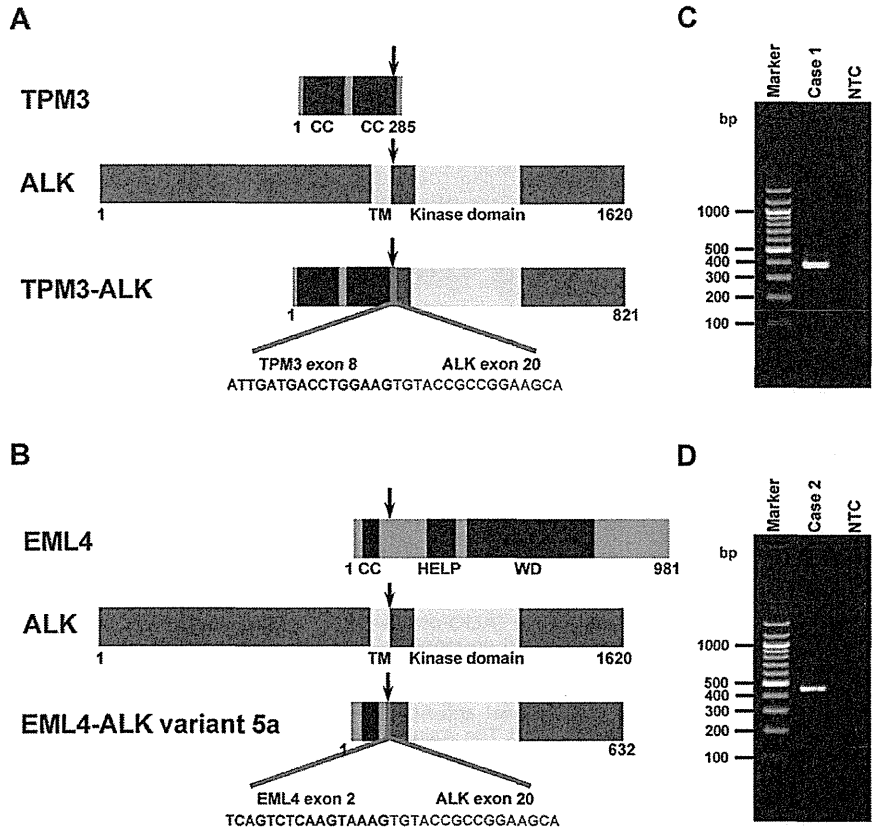

Figure 3. Identification of anaplastic lymphoma kinase (ALK) fusions. Tropomyosin 3 (TPM3) harbors 2 coiled-coil domains. (A) Case 1. A chromosome translocation generates a fusion protein in which the 2 coiled-coil domains of TPM3 and the intracellular region of ALK (containing the tyrosine kinase domain) are conserved. (B) Nucleotide sequencing of the polymerase chain reaction (PCR) products in case 2 revealed that exon 2 of echinoderm microtubule-associated protein like 4 (EML4), comprising a coiled-coil domain, was fused to exon 20 of ALK, generating the variant 5 complementary DNA (cDNA). In TPM3 and EML4 fusions, the region containing the coiled-coil domain is fused to the kinase domain of ALK. Numbers indicate amino acid positions of each protein. Arrow indicates the chromosomal breakpoint. The cDNA fragments of 385 base pairs (bp) and 454 bp were obtained by reverse transcription PCR, corresponding to (C) *TPM3-ALK* and (D) *EML4-ALK* variant 5, respectively. The left lane ("Marker") contains DNA size standards (100-bp ladder). CC indicates coiled-coil domain; HELP, hydrophobic echinoderm microtubule-associated protein; NTC, no-template control; TM, transmembrane domain; WD, WD repeats.

She underwent a translumbar left-radical nephrectomy and is currently alive and well without evidence of disease at 2 years of follow-up.

Case 2

A 53-year-old woman was found incidentally to have microscopic hematuria by medical check-up. Ultrasonography and magnetic resonance imaging showed a change in the left kidney, but the diagnosis was indefinite at that time. One year later, adenocarcinoma cells were detected by urinary cytology, and computed tomography revealed an isodence left renal mass (2.5 cm × 2.5 cm × 2.3 cm). The patient underwent a translumbar left-radical nephrectomy. She is currently alive and well at 7 years after surgery.

The patients had no episodes or family history indicative of sickle cell trait. To the best of our knowledge, there is no reported case of (genetically) Japanese individuals with sickle cell trait/disease.

Histopathological Examinations

The 2 ALK-positive renal cancers were papillary subtype and unclassified (with mixed features of papillary, mucinous cribriform, and solid patterns with rhabdoid cells). They comprised 2.3% of non–clear cell RCCs (2 of 88) and 3.7% of non–clear cell and nonchromophobe RCCs (2 of 54).

Case 1

Histologically, tumor cells were composed of papillary, tubular, or cribriform growth of cuboidal cells with

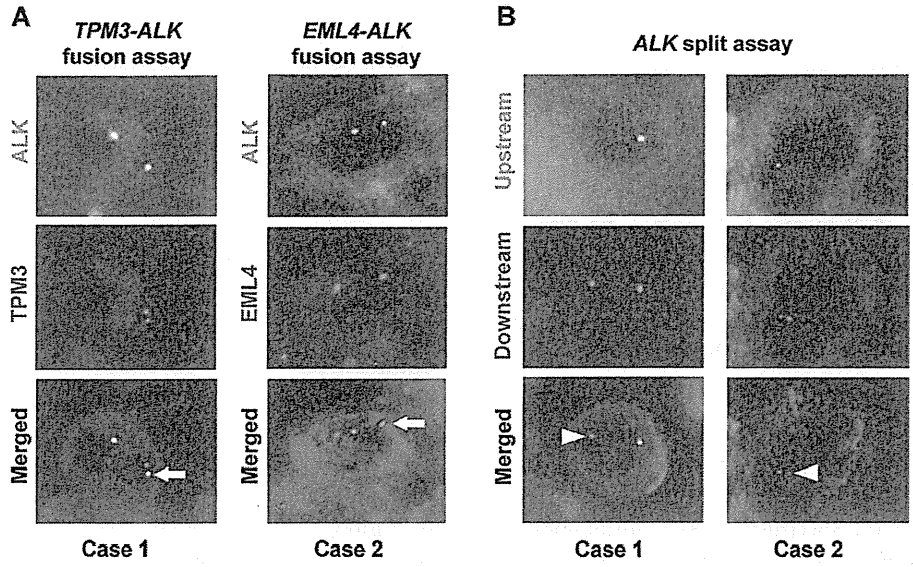

Figure 4. Fluorescence in situ hybridization analyses for *TPM3-ALK* (tropomyosin 3 fusion with anaplastic lymphoma kinase) and *EML4-ALK* (echinoderm microtubule-associated protein like 4 fusion with ALK). (A) In the *TPM3-ALK* and *EML4-ALK* fusion assays, the fusion genes are indicated by arrows. (B) The same clinical specimens as in (A) were subjected to fluorescence in situ hybridization analysis with differentially labeled probes for the upstream (green) or downstream (red) to the ALK breakpoint. In each case, the absence of 1 upstream signal indicated ALK rearrangement. Arrowhead indicates the rearranged ALK. The color of fluorescence for the bacterial artificial chromosome clones and the case numbers are indicated. Nuclei are stained blue with 4′,6-diamidino-2-phenylindole.

eosinophilic cytoplasm. The cribriform morphology consisted of tubular structures with flattened epithelial cells, compressed by mucinous pool and inter- or intracytoplasmic vacuoles. Solid sheets of tumor cells with occasional deeply eosinophilic intracytoplasmic inclusions and eccentric nuclei, resulting in rhabdoid features, were focally identified. Nuclei were round to ovoid, and the nuclear size was basically uniform. Irregular nuclear membranes and nuclear grooves were occasionally observed. Mitotic figures were scant. The background stroma in the tumor area possessed abundant mucin. Frequent deposition of psammoma bodies and infiltration of numerous foamy macrophages were also seen. A large amount of mucinous matrix was highlighted with Alcian blue stain. These histological features resembled the mucinous cribriform pattern frequently observed in ALK-positive lung adenocarcinoma,[18,31] and also a representative case of unclassified RCC by Lopez-Beltran et al,[32] favoring a diagnosis of unclassified RCC. Immunohistochemically, neoplastic cells showed a diffuse and strong positivity for ALK (iAEP), vimentin, EMA, cytokeratin 7, AE1/AE3, cytokeratin CAM5.2, and cytokeratin 34βE12, and focally staining for PAX2, PAX8, AMACR, and CD10. TTF1 and RCC Ma were completely negative. Intracytoplasmic inclusions corresponded to aggregates of intermediate filaments of vimentin. The ALK-staining pattern appeared to be accentuated around the cell membrane of rhabdoid cells. The MIB1 (mindbomb homolog 1) labeling index was less than 1%.

Case 2

Histologically, the tumor consisted of papillary configuration of cuboidal or low columnar cells, with eosinophilic cytoplasm and small uniform round to oval nuclei. A clear cell change was focally seen. Nuclei showed a round to oval shape, and nuclear grooves were frequently observed. The size variation of nuclei was minimal, and the irregularity of the nuclear membrane was evident. Nuclear pseudoinclusions were seldom seen. Small nucleoli were occasionally identified, but mitoses were absent. The fibrovascular cores of papillary architecture contained numerous psammoma bodies and foamy macrophages. In addition, glandular lumens of tumor cells focally contained myxoid materials. These findings morphologically corresponded to papillary RCC, but did not fit to types 1 and 2 by the classification of Delahunt and Eble.[33] In contrast, the features resembled papillary RCC, type 2A, described by Yang et al.[34] Alcian blue stain highlighted a small amount of stromal-type mucin. Upon immunohistochemical analysis, neoplastic cells were diffusely and

strongly positive for ALK (iAEP), vimentin, EMA, cytokeratin 7, AE1/AE3, cytokeratin CAM5.2, cytokeratin 34βE12, and AMACR, and focally positive for PAX2 and PAX8, but negative for TTF1, CD10, and RCC Ma.

Examinations of Other Gene Aberrations

For *MET*, a cDNA fragment with the predicted size was obtained by RT-PCR in case 1. In case 2, no products were identified, indicating that the tumor of the patient did not express *MET*. No mutations were identified in case 1 by sequencing. TFE3 split signals were not observed in either of the 2 cases by FISH.

DISCUSSION

Recently, 2 independent groups have reported vinculin-ALK (VCL-ALK) in renal cancer (Table 1).[35,36] These findings broaden the spectrum of ALK fusion–positive tumors. Interestingly, the 2 patients described in the reports share several uncommon backgrounds for renal cancer: very early onset (6- and 16-year-old boys), a history of sickle cell trait, and uncommon histopathological subtypes (medullary subtype and indeterminate subtype with mixed features of medullary, chromophobe, and transitional cell subtypes). In this study, we screened 355 renal tumors, including 343 RCCs, and identified ALK fusions in 2 RCCs. Significantly, we identified ALK fusions in adult patients (36- and 53-year-old females) without sickle cell trait. This finding will provide a key to ALK inhibitor therapy for more common renal cancers.

RCC associated with *TFE3* gene fusions is already a distinctive entity in the World Health Organization classification,[37,38] and *MET* mutation has been described in 13% of sporadic papillary RCCs.[39] In the present study, we identified neither *MET* nor *TFE3* aberrations in our ALK-positive renal cancer cases. *ALK* rearrangements are recognized as almost mutually exclusive to other mutations such as *EGFR* (epidermal growth factor receptor) and *KRAS* (v-Ki-ras2 Kirsten rat sarcoma viral oncogene) in lung cancer.[6,40] All of the tumor cells in the 2 ALK-positive renal cancers observed by immunohistochemistry expressed ALK fusion protein, suggesting that all tumor cells harbor one or more *ALK* fusion genes. Therefore, as well as other ALK-positive tumors, *ALK* rearrangement in renal cancer probably occurs at a very early phase of carcinogenesis, and is likely to be a driver mutation and mutually exclusive to other driver mutations. As in the case of ALK-positive ALCL, ALK-positive renal cancer will be a distinct molecular pathological entity.

TPM3-ALK was first identified in ALCL in 1999,[41] and subsequently found in IMT in 2000.[5] Therefore, RCC is the third type of cancer that may harbor TPM3-ALK. The organ distribution of EML4-ALK is somewhat controversial. Since its discovery, EML4-ALK has been reported to be identified in lung, breast, and colon cancers. Many research groups have reported the presence of EML4-ALK in a small subset of lung adenocarcinomas (2%-10%). Interestingly, a group in the United States reported the presence of EML4-ALK in breast (5 of 209) and colorectal (2 of 83) cancers, identified by RT-PCR optimized for variants 1, 2, and 3, without showing histopathological evidence.[42] In contrast, 2 Japanese groups examined these cancers (90 breast and 96 colon cancers by RT-PCR for EML4-ALK variants 1 and 2, and 48 breast and 50 colon cancers by multiplex RT-PCR for all possible fusions), but detected no positive cases.[30,43] One possible reason for this discrepancy may be differences in ethnicity. In the present study, we showed histopathological features of the 2 ALK-positive renal cancers. In addition to morphology, the positivity of PAX2 and PAX8 and the negativity of TTF1 strongly indicated that the ALK-positive cancers of the present cases were primary RCCs, and not metastatic lesions of ALK-positive lung cancer.

The oncogenic activities of TPM3-ALK and EML4-ALK have previously been documented,[30,44] and therefore we did not demonstrate them in the present study. As in the case of other ALK-positive tumors, ALK-positive renal cancer is a promising candidate disease for ALK inhibitor therapy. In the present study, we screened surgically removable cases; the prognoses for the 2 ALK-positive patients were good, without recurrence. To realize the full potential of ALK inhibitors in renal cancers, it is important to identify the detailed clinicopathological features of ALK-positive cases, especially those of advanced or recurrent cases, by large-scale screening. For this purpose, anti-ALK immunohistochemistry can most readily be carried out as a primary screening tool. However, caution is needed; the screening immunohistochemical assay should be appropriately sensitive, because our present findings indicate that renal cancer involves EML4-ALK, which is barely detectable by conventional immunohistochemistry methods.[13,45]

Is morphology a clue to the presence of ALK fusion in renal cancers? Almost all ALK-positive lung cancers are adenocarcinomas, and more frequently show mucinous cribriform patterns and signet-ring cells than do ALK-negative adenocarcinomas.[18,31,46] ALK fusion is probably very rare in clear cell RCC, which is the most common

Table 1. ALK-Positive Renal Cancers: Present Cases and Review of Literature

Characteristic	VCL-ALK (Debelenko et al[36])	VCL-ALK (Marino-Enriquez et al[35])	TPM3-ALK (Case 1)	EML4-ALK (Case 2)
Age, y	16	6	36	53
Sex	Male	Male	Female	Female
Ethnicity	African American	African American	Japanese	Japanese
Past history	Sickle cell trait	Sickle cell trait	Tuberculosis (22 y old)	Pleomorphic adenoma (50 y old)
Karyotype	Abnormal complex karyotype	46,XY,t(2;10)(p23;q22), add(14)(p11)	Not examined	Not examined
Symptom	Right flank pain, gross hematuria	Intermittent periumbilical pain, hematuria	Pyelonephritis	Microscopic hematuria
Stage	Stage III	Stage I	Stage I	Stage I
Follow-up	9 mo, alive. No evidence of disease	21 mo, alive. No evidence of disease	2 y, alive. No evidence of disease	3 y, alive. No evidence of disease
Gross findings	6.5-cm irregularly shaped solid tumor mass with infiltrative borders centered in the right renal medulla	4.5-cm irregularly spherical mass with lobulated, fleshy light tan appearance centered in the medulla	4.0 cm × 4.0 cm × 3.5 cm irregularly shaped solid tumor with expansive borders centered in the cortex	Double cancer. A: 2.5 cm × 2.5 cm ×2.3 cm solid yellow tumor in the cortex of the left intermediate pole. B: 0.6-cm yellow mass in the cortex of the left inferior pole
Microscopic findings	Diffuse sheet-like pattern; round, oval, and polygonal tumor cells; eosinophilic cytoplasm; moderately polymorphic and vesicular nuclei	Solid growth pattern; spindle-shaped cells with large vesicular nuclei; clear coarse chromatin and abundant eosinophilic cytoplasm	Papillary, tubular, or cribriform growth of cuboidal cells with eosinophilic cytoplasm. Nuclei round to ovoid; nuclear size basically uniform	A: Papillary structure of cuboidal or low columnar cells with eosinophilic cytoplasm and small uniform round to oval nuclei. B: Clear cell
Immunohistochemistry	Positive: AE1/AE3, CAM5.2, CK7, EMA, INI1, TFE3. Negative: CD10, S100, HMB45, WT1	Positive: AE1/AE3, CAM5.2, EMA	Positive: ALK, vimentin, EMA, cytokeratin 7, AE1/AE3, CAM5.2, 34βE12, AMACR (focal), CD10 (focal), PAX2 (focal), PAX8 (focal). Negative: TTF1, RCC Ma	A: Positive: ALK, vimentin, EMA, cytokeratin 7, AE1/AE3, CAM5.2, 34βE12, AMACR, PAX2 (focal), PAX8 (focal). Negative: CD10, TTF1, RCC Ma
Diagnosis	Renal cell carcinoma, indeterminate subtype (medullary, chromophobe, transitional cell carcinoma mixed)	Renal medullary carcinoma	Renal cell carcinoma, unclassified	A: Papillary renal cell carcinoma, type 2A. B: Clear cell renal cell carcinoma

ALK indicates anaplastic lymphoma kinase; EML4, echinoderm microtubule–associated protein like 4; TPM3, tropomyosin 3; VCL, vinculin.

subtype of renal cancer; 2 previously reported cases with VCL-ALK were not clear cell RCC,[35,36] and we identified no ALK-positive cases in 255 clear cell RCCs in this study. Interestingly, case 1 showed a mucinous cribriform pattern. This may be a characteristic feature of ALK-positive carcinomas, universally applicable to carcinomas of various organs. Further study with a larger number of cases is warranted.

Molecular-targeted therapy of advanced renal cancers is starting to realize its full potential. However, complete remission is rarely achieved, because no agent targets a key molecule associated with "oncogene addiction" of renal cancer. In this context, ALK fusion constitutes a promising advance in renal cancers, as has previously been demonstrated with various other types of cancer. In the present study, we identified 2 adult cases of ALK-positive renal cancer in patients without uncommon backgrounds. Our findings confirm the potential of ALK inhibitor therapy for RCC. More detailed clinicopathological features of ALK-positive renal cancers, especially at higher clinical stages, are desirable. Hunting the "ALKoma" in various types of carcinomas, as well as in lung and kidney cancer, will provide an answer to these pathological and clinical questions.

FUNDING SOURCES

This work was supported in part by Grants-in-Aid for Scientific Research from the Ministry of Education, Culture, Sports, Science, and Technology of Japan as well as by grants from the Japan Society for the Promotion of Science; the Ministry of Health, Labour, and Welfare of Japan; the Vehicle Racing Commemorative Foundation of Japan; Princess Takamatsu Cancer Research Fund; and the Uehara Memorial Foundation.

CONFLICT OF INTEREST DISCLOSURE

Dr. Takeuchi is a scientific advisor for the anti-ALK iAEP immunohistochemistry kit (ALK Detection Kit, Nichirei Bioscience, Tokyo, Japan). All remaining authors have made no disclosures.

REFERENCES

1. International Agency for Research on Cancer. The GLOBOCAN Project: GLOBOCAN 2008. http://globocan.iarc.fr/. Accessed December 16, 2011.
2. Campbell SC, Novick AC, Bukowski RM. Renal tumors. In: Wein AJ, Kavoussi LR, Novick AC, Partin AW, Peters CA, eds. Campbell-Walsh Urology. 9th ed. Philadelphia, PA: Saunders; 2007: 1567-1637.
3. Morris SW, Kirstein MN, Valentine MB, et al. Fusion of a kinase gene, ALK, to a nucleolar protein gene, NPM, in non-Hodgkin's lymphoma. *Science.* 1994;263:1281-1284.
4. Shiota M, Fujimoto J, Semba T, Satoh H, Yamamoto T, Mori S. Hyperphosphorylation of a novel 80 kDa protein-tyrosine kinase similar to Ltk in a human Ki-1 lymphoma cell line, AMS3. *Oncogene.* 1994;9:1567-1574.
5. Lawrence B, Perez-Atayde A, Hibbard MK, et al. TPM3-ALK and TPM4-ALK oncogenes in inflammatory myofibroblastic tumors. *Am J Pathol.* 2000;157:377-384.
6. Soda M, Choi YL, Enomoto M, et al. Identification of the transforming EML4-ALK fusion gene in non-small-cell lung cancer. *Nature.* 2007;448:561-566.
7. Rikova K, Guo A, Zeng Q, et al. Global survey of phosphotyrosine signaling identifies oncogenic kinases in lung cancer. *Cell.* 2007; 131:1190-1203.
8. Soda M, Takada S, Takeuchi K, et al. A mouse model for EML4-ALK-positive lung cancer. *Proc Natl Acad Sci U S A.* 2008;105: 19893-19897.
9. Kwak EL, Bang YJ, Camidge DR, et al. Anaplastic lymphoma kinase inhibition in non-small-cell lung cancer. *N Engl J Med.* 2010;363:1693-1703.
10. Chihara D, Suzuki R. More on crizotinib. *N Engl J Med.* 2011;364: 776-777.
11. Butrynski JE, D'Adamo DR, Hornick JL, et al. Crizotinib in ALK-rearranged inflammatory myofibroblastic tumor. *N Engl J Med.* 2010;363:1727-1733.
12. Gambacorti-Passerini C, Messa C, Pogliani EM. Crizotinib in anaplastic large-cell lymphoma. *N Engl J Med.* 2011;364:775-776.
13. Takeuchi K, Choi YL, Togashi Y, et al. KIF5B-ALK, a novel fusion oncokinase identified by an immunohistochemistry-based diagnostic system for ALK-positive lung cancer. *Clin Cancer Res.* 2009;15: 3143-3149.
14. Martelli MP, Sozzi G, Hernandez L, et al. EML4-ALK rearrangement in non-small cell lung cancer and non-tumor lung tissues. *Am J Pathol.* 2009;174:661-670.
15. Jokoji R, Yamasaki T, Minami S, et al. Combination of morphological feature analysis and immunohistochemistry is useful for screening of EML4-ALK-positive lung adenocarcinoma. *J Clin Pathol.* 2010;63:1066-1070.
16. Kijima T, Takeuchi K, Tetsumoto S, et al. Favorable response to crizotinib in three patients with echinoderm microtubule-associated protein-like 4-anaplastic lymphoma kinase fusion-type oncogene-positive non-small cell lung cancer. *Cancer Sci.* 2011;102:1602-1604.
17. Kimura H, Nakajima T, Takeuchi K, et al. ALK fusion gene positive lung cancer and 3 cases treated with an inhibitor for ALK kinase activity. *Lung Cancer.* 2012;75:66-72.
18. Yoshida A, Tsuta K, Nakamura H, et al. Comprehensive histologic analysis of ALK-rearranged lung carcinomas. *Am J Surg Pathol.* 2011;35:1226-1234.
19. Yi ES, Boland JM, Maleszewski JJ, et al. Correlation of IHC and FISH for ALK gene rearrangement in non-small cell lung carcinoma: IHC score algorithm for FISH. *J Thorac Oncol.* 2011;6:459-465.
20. Kudo K, Takeuchi K, Tanaka H, et al. Immunohistochemical screening of ALK lung cancer with biopsy specimens of advanced lung cancer. *J Clin Oncol.* 2010;28(suppl): (abstract 10532).
21. Sakairi Y, Nakajima T, Yasufuku K, et al. EML4-ALK fusion gene assessment using metastatic lymph node samples obtained by endobronchial ultrasound-guided transbronchial needle aspiration. *Clin Cancer Res.* 2010;16:4938-4945.
22. Nakajima T, Kimura H, Takeuchi K, et al. Treatment of lung cancer with an ALK Inhibitor after EML4-ALK fusion gene detection using endobronchial ultrasound-guided transbronchial needle aspiration. *J Thorac Oncol.* 2010;5:2041-2043.
23. Takeuchi K, Soda M, Togashi Y, et al. Identification of a novel fusion, SQSTM1-ALK, in ALK-positive large B-cell lymphoma. *Haematologica.* 2011;96:464-467.
24. Takeuchi K, Soda M, Togashi Y, et al. Pulmonary inflammatory myofibroblastic tumor expressing a novel fusion, PPFIBP1-ALK: reappraisal of anti-ALK immunohistochemistry as a tool for novel ALK-fusion identification. *Clin Cancer Res.* 2011;17:3341-3348.
25. Shiota M, Fujimoto J, Takenaga M, et al. Diagnosis of t(2;5)(p23;q35)-associated Ki-1 lymphoma with immunohistochemistry. *Blood.* 1994;84:3648-3652.
26. Pulford K, Lamant L, Morris SW, et al. Detection of anaplastic lymphoma kinase (ALK) and nucleolar protein nucleophosmin (NPM)-ALK proteins in normal and neoplastic cells with the monoclonal antibody ALK1. *Blood.* 1997;89:1394-1404.
27. Shiota M, Nakamura S, Ichinohasama R, et al. Anaplastic large cell lymphomas expressing the novel chimeric protein p80NPM/ALK: a distinct clinicopathologic entity. *Blood.* 1995;86:1954-1960.
28. Delsol G, Lamant L, Mariamé B, et al. A new subtype of large B-cell lymphoma expressing the ALK kinase and lacking the 2; 5 translocation. *Blood.* 1997;89:1483-1490.
29. Lamant L, Pulford K, Bischof D, et al. Expression of the ALK tyrosine kinase gene in neuroblastoma. *Am J Pathol.* 2000;156:1711-1721.
30. Takeuchi K, Choi YL, Soda M, et al. Multiplex reverse transcription-PCR screening for EML4-ALK fusion transcripts. *Clin Cancer Res.* 2008;14:6618-6624.
31. Inamura K, Takeuchi K, Togashi Y, et al. EML4-ALK fusion is linked to histological characteristics in a subset of lung cancers. *J Thorac Oncol.* 2008;3:13-17.
32. Lopez-Beltran A, Carrasco JC, Cheng L, Scarpelli M, Kirkali Z, Montironi R. 2009 update on the classification of renal epithelial tumors in adults. *Int J Urol.* 2009;16:432–443.
33. Delahunt B, Eble JN. Papillary renal cell carcinoma: a clinicopathologic and immunohistochemical study of 105 tumors. *Mod Pathol.* 1997;10:537-544.
34. Yang XJ, Tan MH, Kim HL, et al. A molecular classification of papillary renal cell carcinoma. *Cancer Res.* 2005;65:5628-5637.
35. Mariño-Enríquez A, Ou WB, Weldon CB, Fletcher JA, Pérez-Atayde AR. ALK rearrangement in sickle cell trait-associated renal medullary carcinoma. *Genes Chromosomes Cancer.* 2011;50:146-153.
36. Debelenko LV, Raimondi SC, Daw N, et al. Renal cell carcinoma with novel VCL-ALK fusion: new representative of ALK-associated tumor spectrum. *Mod Pathol.* 2011;24:430-442.
37. Argani P, Ladanyi M. Renal carcinomas associated with Xp11.2 translocations/TFE3 gene fusions. In: Eble J, Sauter G, Epstein J, Sesterhenn I, eds. Pathology and Genetics of Tumours of the Urinary System and Male Genital Organs. Lyon, France: IARC Press; 2004:37-38.
38. Ross H, Argani P. Xp11 translocation renal cell carcinoma. *Pathology.* 2010;42:369-373.

39. Schmidt L, Junker K, Nakaigawa N, et al. Novel mutations of the MET proto-oncogene in papillary renal carcinomas. *Oncogene.* 1999; 18:2343-2350.
40. Inamura K, Takeuchi K, Togashi Y, et al. EML4-ALK lung cancers are characterized by rare other mutations, a TTF-1 cell lineage, an acinar histology, and young onset. *Mod Pathol.* 2009;22:508-515.
41. Lamant L, Dastugue N, Pulford K, Delsol G, Mariamé B. A new fusion gene TPM3-ALK in anaplastic large cell lymphoma created by a (1;2)(q25;p23) translocation. *Blood.* 1999;93: 3088-3095.
42. Lin E, Li L, Guan Y, et al. Exon array profiling detects EML4-ALK fusion in breast, colorectal, and non-small cell lung cancers. *Mol Cancer Res.* 2009;7:1466-1476.
43. Fukuyoshi Y, Inoue H, Kita Y, Utsunomiya T, Ishida T, Mori M. EML4-ALK fusion transcript is not found in gastrointestinal and breast cancers. *Br J Cancer.* 2008;98:1536-1539.
44. Giuriato S, Faumont N, Bousquet E, et al. Development of a conditional bioluminescent transplant model for TPM3-ALK-induced tumorigenesis as a tool to validate ALK-dependent cancer targeted therapy. *Cancer Biol Ther.* 2007;6:1318-1323.
45. Sozzi G, Martelli MP, Conte D, et al. The EML4-ALK transcript but not the fusion protein can be expressed in reactive and neoplastic lymphoid tissues. *Haematologica.* 2009;94:1307-1311.
46. Rodig SJ, Mino-Kenudson M, Dacic S, et al. Unique clinicopathologic features characterize ALK-rearranged lung adenocarcinoma in the western population. *Clin Cancer Res.* 2009;15:5216-5223.

MODERN PATHOLOGY (2012) 25, 1574–1583

Reproducibility of histopathological subtypes and invasion in pulmonary adenocarcinoma. An international interobserver study

Erik Thunnissen[1], Mary Beth Beasley[2], Alain C Borczuk[3], Elisabeth Brambilla[4], Lucian R Chirieac[5], Sanja Dacic[6], Douglas Flieder[7], Adi Gazdar[8], Kim Geisinger[9], Philip Hasleton[10], Yuichi Ishikawa[11], Keith M Kerr[12], Sylvie Lantejoul[4], Yoshiro Matsuno[13], Yuko Minami[13], Andre L Moreira[14], Noriko Motoi[11], Andrew G Nicholson[15], Masayuki Noguchi[13], Daisuke Nonaka[16], Giuseppe Pelosi[17], Iver Petersen[18], Natasha Rekhtman[14], Victor Roggli[19], William D Travis[14], Ming S Tsao[20], Ignacio Wistuba[21], Haodong Xu[22], Yasushi Yatabe[23], Maureen Zakowski[14], Birgit Witte[24] and Dirk Joop Kuik[24]

[1]Department of Pathology, VU University Medical Centre, Amsterdam, The Netherlands; [2]Mount Sinai Hospital, New York, NY, USA; [3]Department of Pathology, Anatomic Pathology Columbia University Medical Center, New York, NY, USA; [4]Department of Pathology, CHU A Michallon, INSERM U 823-Institut A Bonniot-University J Fourier, Grenoble, France; [5]Department of Pathology, Brigham and Women's Hospital, Boston, MA, USA; [6]Department of Pathology, University of Pittsburgh, Pittsburgh, PA, USA; [7]Department of Pathology, Fox Chase Cancer Center, Philadelphia, PA, USA; [8]UT Southwestern Medical Center, Dallas, TX, USA; [9]Piedmont Pathology Associates, Hickory, NC, USA; [10]Department of Pathology, Hadassah Hospital, Jerusalem, Israel; [11]Division of Pathology, The Cancer Institute, Japanese Foundation for Cancer Research, Tokyo, Japan; [12]Department of Pathology, Aberdeen Royal Infirmary, Aberdeen, UK; [13]Department of Pathology, Faculty of Medicine, University of Tsukuba, Tsukuba, Japan; [14]Department of Pathology, Memorial Sloan Kettering Cancer Center, New York, NY, USA; [15]Department of Histopathology, Royal Brompton Hospital, London, UK; [16]Department of Histopathology, The Christie NHS Foundation, Manchester, UK; [17]Department of Pathology and Laboratory Medicine, Fondazione IRCCS Istituto Nazionale dei Tumori and Università degli Studi di Milano, Milan, Italy; [18]Institute of Pathology, Jena University Hospital, Friedrich-Schiller-University, Jena, Germany; [19]DUMC 3712, Durham, NC, USA; [20]Department of Pathology, University Health Network-Princess Margaret Hospital and University of Toronto, Toronto, Canada; [21]Department of Pathology, University of Texas MD Anderson Cancer Center, Houston, TX, USA; [22]Department of Pathology and Laboratory Medicine, Aab Cardiovascular Research Institute, University of Rochester Medical Center, Rochester, NY, USA; [23]Department of Pathology and Molecular Diagnostics, Aichi Cancer Center, Nagoya, Japan and [24]Department of Epidemiology and Biostatistics, VU University Medical Centre, Amsterdam, The Netherlands

Histological subtyping of pulmonary adenocarcinoma has recently been updated based on predominant pattern, but data on reproducibility are required for validation. This study first assesses reproducibility in subtyping adenocarcinomas and then assesses further the distinction between invasive and non-invasive (wholly lepidic) pattern of adenocarcinoma, among an international group of pulmonary pathologists. Two ring studies were performed using a micro-photographic image-based method, evaluating selected images of lung adenocarcinoma histologic patterns. In the first study, 26 pathologists reviewed representative images of typical and 'difficult' histologic patterns. A total number of scores for the typical patterns combined ($n=94$) and

Correspondence: Dr E Thunnissen, MD, PhD, Department of Pathology, VU University Hospital, De Boelelaan 1117, 1081 HV Amsterdam, The Netherlands.
E-mail: e.thunnissen@vumc.nl
Received 12 February 2012; revised 9 April 2012; accepted 15 April 2012; published online 20 July 2012

the difficult cases ($n=21$) were 2444 and 546, respectively. The mean kappa score (±s.d.) for the five typical patterns combined and for difficult cases were 0.77±0.07 and 0.38±0.14, respectively. Although 70% of the observers identified 12–65% of typical images as single pattern, highest for solid and least for micropapillary, recognizing the predominant pattern was achieved in 92–100%, of the images except for micropapillary pattern (62%). For the second study on invasion, identified as a key problem area from the first study, 28 pathologists submitted and reviewed 64 images representing typical as well as 'difficult' examples. The kappa for typical and difficult cases was 0.55±0.06 and 0.08±0.02, respectively, with consistent subdivision by the same pathologists into invasive and non-invasive categories, due to differing interpretation of terminology defining invasion. In pulmonary adenocarcinomas with classic morphology, which comprise the majority of cases, there is good reproducibility in identifying a predominant pattern and fair reproducibility distinguishing invasive from *in-situ* (wholly lepidic) patterns. However, more precise definitions and better education on interpretation of existing terminology are required to improve recognition of purely *in-situ* disease, this being an area of increasing importance.
Modern Pathology (2012) **25,** 1574–1583; doi:10.1038/modpathol.2012.106; published online 20 July 2012

Keywords: adenocarcinoma; histopathology; invasion; lung; reproducibility; subtyping

The 2004 WHO classification of lung cancer contained four major patterns of adenocarcinoma: bronchioloalveolar, acinar, papillary and solid pattern with the most common pattern consisting of a mixture of these four subtypes.[1] In the recent IASLC/ATS/ERS lung adenocarcinoma classification several major changes are made.[2] First, the mixed subtype category is discontinued and tumors are subtyped according to the predominant pattern following a comprehensive semiquantitatively estimating the percentage of each of the adenocarcinoma histologic patterns. However, evidence for use of predominant patterns to improve reproducibility pattern diagnosis was at the time not available. Therefore, this was put forth as a weak recommendation with low quality of evidence (Pathology Recommendation 4).[1] Second, the term bronchioloalveolar carcinoma (BAC) is no longer used, as BAC was being interpreted in four different ways: (1) adenocarcinoma *in situ*, (2) minimally invasive adenocarcinoma, (3) overtly invasive adenocarcinoma with a lepidic pattern and (4) invasive mucinous adenocarcinoma (formerly mucinous BAC). In addition, micropapillary adenocarcinoma was added as a fifth major pattern due to its association with poor prognosis.[3,4] Diagnostic inconsistencies may originate from difficulties in interpretation due to subjective application of existing criteria.

In the past, the distinction between small-cell and non-small-cell lung cancers has been shown to have high accuracy and reproducibility.[5,6] Also, in resection specimen, accuracy in distinguishing squamous cell carcinoma from adenocarcinoma has been repeatedly demonstrated, even though cases that are difficult to classify by morphology alone may remain in poorly differentiated tumors.[5–10] However, there remains a lack of data on reproducibility in relation to identifying predominant patterns of adenocarcinoma.

The intention of this study was therefore to assess the reproducibility of histopathological subtyping for adenocarcinomas among pulmonary pathologists from three continents, with respect to both 'histologic patterns' and 'invasion'.

Materials and methods

To assess reproducibility of adenocarcinoma subtyping, two ring studies were performed. In the first study, 19 pathologists were asked to submit six cases, consisting of micro-photomicrographs, pasted into a PowerPoint slide. Five of the six cases represent one example each of the five typical histological patterns of adenocarcinoma: acinar, non-mucinous lepidic (formerly BAC), micropapillary, papillary and solid pattern, as perceived by the contributing pathologist.[1] The sixth case was regarded as a difficult case by the contributing pathologist. The PowerPoint slide contained two images: the left sided one very-low-magnification picture (objective 2 to ×4) to represent the general architectural pattern, and the right side one showing a higher magnification (objective ×10, or minimally four sizes of 'normal' alveolar spaces in the longest axis of the image) to highlight the diagnostic area to be evaluated. The assumption was made that assessments would be made only on the high-magnification images. Cases ($n=115$) were randomized and blinded to participants who classified cases by their dominant pattern; if more than one pattern was recognized, then additional pattern(s) were provided additionally (Table 1).

After the first round, participants felt that difficult cases were centered on the concept of 'invasion' (distinguishing pure lepidic pattern from others), which led to the initiation of a second ring study. For the second study, 10 pathologists submitted photomicrographs in similar manner as before, but to show typical invasion ($n=20$), no invasion ($n=20$) and 'problem cases' ($n=24$). All cases were randomized (JK) and for each case

Table 1 CRF contains the possible categories for diagnosing the case(s)

1	Pathologist study number	[.]
	Diagnosis	[.] one of the numbers 2–71
2	AC pure	
3	BA pure	
4	MP pure	
5	PA pure	
6	SO pure	
7	AC predominant with BA	
8	AC predominant with MP	
9	AC predominant with PA	
10	AC predominant with SO	
11	AC predominant with BA and MP	
12	AC predominant with MP and PA	
13	AC predominant with PA and SO	
14	AC predominant with SO and BA	
15	AC predominant with BA and MP and PA	
16	AC predominant with MP and PA and SO	
17	AC predominant with PA and SO and BA	
18	AC predominant with SO and BA and MP	
19	AC predominant with BA and MP and PA and SO	
20	BA predominant with MP	
21	BA predominant with PA	
22	BA predominant with SO	
23	BA predominant with AC	
24	BA predominant with MP and PA	
25	BA predominant with PA and SO	
26	BA predominant with SO and AC	
27	BA predominant with AC and MP	
28	BA predominant with MP and PA and SO	
29	BA predominant with PA and SO and AC	
30	BA predominant with SO and AC and MP	
31	BA predominant with AC and MP and PA	
32	BA predominant with MP and PA and SO and AC	
33	MP predominant with PA	
34	MP predominant with SO	
35	MP predominant with AC	
36	MP predominant with BA	
37	MP predominant with PA and SO	
38	MP predominant with SO and AC	
39	MP predominant with AC and BA	
40	MP predominant with BA and PA	
41	MP predominant with PA and SO and AC	
42	MP predominant with SO and AC and BA	
43	MP predominant with AC and BA and PA	
44	MP predominant with BA and PA and SO	
45	MP predominant with PA and SO and AC and BA	
46	PA predominant with SO	
47	PA predominant with AC	
48	PA predominant with BA	
49	PA predominant with MP	
50	PA predominant with SO and AC	
51	PA predominant with AC and BA	
52	PA predominant with BA and MP	
53	PA predominant with MP and SO	
54	PA predominant with SO and AC and BA	
55	PA predominant with AC and BA and MP	
56	PA predominant with BA and MP and SO	
57	PA predominant with MP and SO and AC	
58	PA predominant with SO and AC and BA and MP	
59	SO predominant with AC	
60	SO predominant with BA	
61	SO predominant with MP	
62	SO predominant with PA	
63	SO predominant with AC and BA	
64	SO predominant with BA and MP	
65	SO predominant with MP and PA	
66	SO predominant with PA and AC	
67	SO predominant with AC and BA and MP	
68	SO predominant with BA and MP and PA	
69	SO predominant with MP and PA and AC	
70	SO predominant with PA and AC and BA	
71	SO predominant with AC and BA and MP and PA	
The amount of certainty is defined as follows 72 = certain of diagnosis 73 = probable, consult colleague 74 = uncertain, consult colleague		
AMOUNT of certainty		[.] one of the numbers 72–74

AC, acinar; BA, bronchioloalveolar; CRF, case report form; MP, micropapillary; PA, papillary; SO, solid.
As it is not excluded that an image may contain in the eye of a 'blinded' reader more than one pattern, all possible perturbations for diagnosis are numbered individually. If two patterns are equally present, please make choice of one of the predominant options.

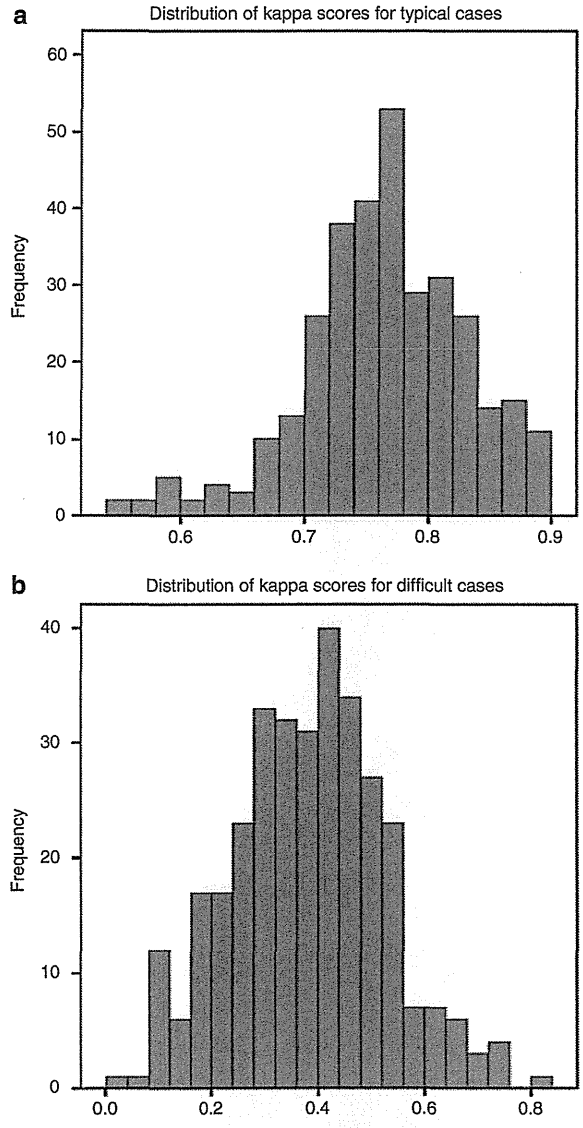

Figure 1 Distribution of kappa scores between all pairs of pathologists for typical cases (**a**) and difficult (**b**) cases.

the reviewer were asked to provide a 'score' on invasion using five categories: invasion, definite or probable, no invasion, definite or probable, and undetermined.

Statistical Analysis

Kappa score was calculated for the typical cases (separately for five typical patterns and typical invasion) and difficult cases (separately for patterns and invasion) by comparing the scores of submitting pathologist with the 'blind' reading of 26 pathologists. For difficult cases, kappa score was calculated for combinations of all pathologists. For the pattern subtyping a dominant and a subscore were calculated for each case and pathologist. The subscore for each subpattern (=non-dominant histologic pattern) was 32, 24, 20 or 16 in case of 1, 2, 3 or 4 subpatterns. The dominant pattern received 512 points minus the number of subpatterns times the subscore. The total score for each pattern was obtained by summing the scores over all pathologists. The overall dominant score for each case was then defined as the highest total score divided by

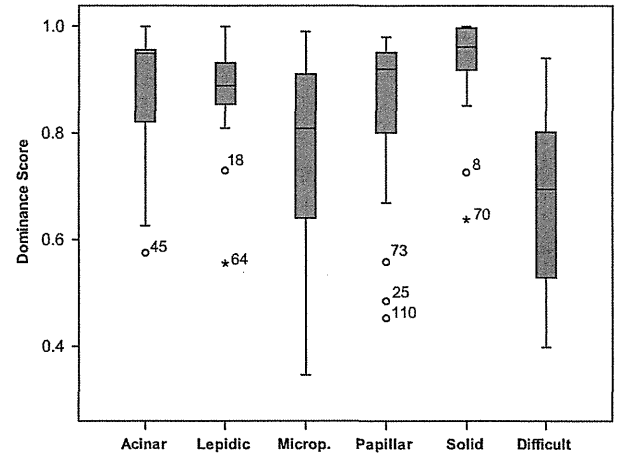

Figure 2 Box plot distribution of the dominant pattern score (1=perfect agreement, 0=no agreement) is shown for the 'typical' patterns according to the submitting pathologist for each of the five histologic subtypes: acinar, lepidic, microp(apillary), papillary and solid. Note that box represents interquartile range (IQR), line in the box is median, wiskers 1.5 × IQR and occasional outliers (o,*) are numbered cases.

Table 2 Cross table of 5 patterns of adenocarcinoma subclassification denoting overlap areas of the diagnostic scores (in percentages) with more than one pattern

Pattern	*Acinar (%)*	*Lepidic (%)*	*Micropapillary (%)*	*Papillary (%)*	*Solid (%)*
Lepidic	9				
Micropapillary	6	6			
Papillary	14	10	22		
Solid	15	0	3	2	
Total/pattern	44	25	37	48	20

Table 3 The number of pathologists among 26, who scored at least 70% of the cases correctly as a single pattern or predominant pattern

Submitted pattern	*Single pattern (%)*	*Predominant pattern (%)*
Acinar ($n=20$)	17/26 (65)	25/26 (96)
Lepidic (BAC; $n=19$)	11/26 (42)	24/26 (92)
Micropapillary ($n=16$)	3/26 (12)	16/26 (62)
Papillary ($n=19$)	5/26 (19)	25/26 (96)
Solid ($n=20$)	17/26 (65)	26/26 (100)

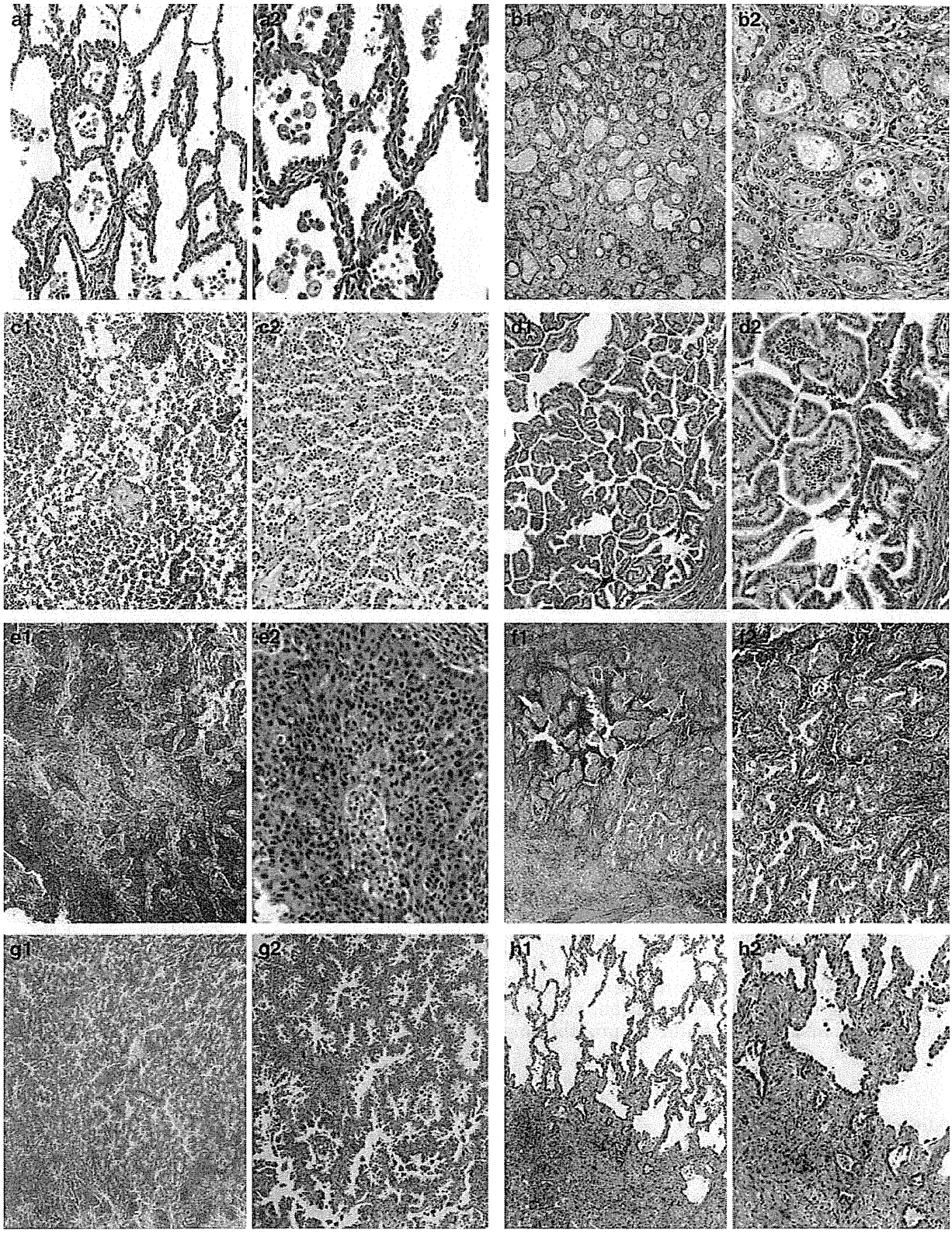

Figure 3 Examples of unanimous lepidic (**a**), acinar (**b**), micropapillary (**c**), papillary (**d**) and solid (**e**) pattern are shown, as well as examples of more than one pattern with percent of pathologists recording that pattern (with judgement on second image, **f–j**). Patterns scored by >10% of the pathologists are mentioned. **f**: overlap solid (96%), acinar (93%), micropapillary (15%), papillary (15%); **g**: overlap micropapillary (96%), papillary (11%); **h**: overlap AIS (92%), acinar (78%); **i**: overlap AIS (78%), papillary (54%); **j**: overlap AIS (66%), micropapillary (42%), papillary (30%) and acinar (27%).

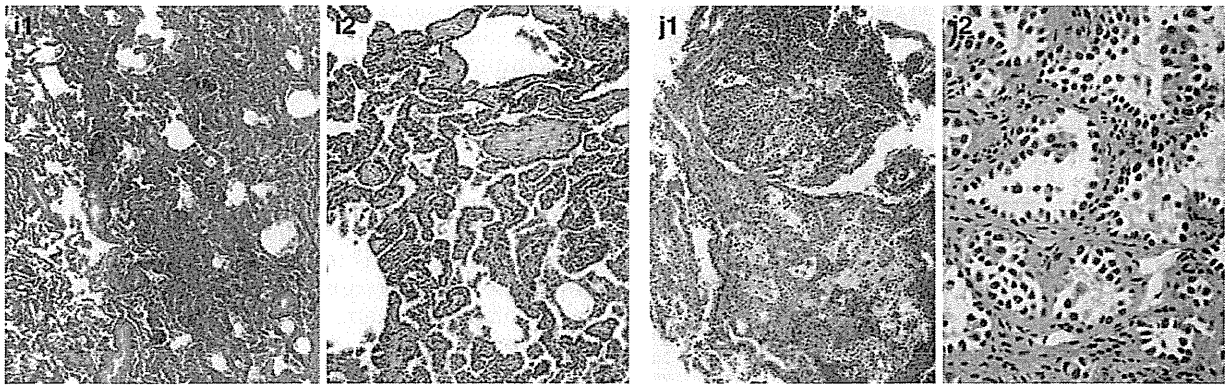

Figure 3 Continued.

the sum of all total scores. For each 'typical' pattern, the number of cases where 70 of the pathologists scored a submitted pattern as single or a predominant pattern were also calculated.

In the second study on 'invasion', kappa was analyzed for five and three categories. For each case an invasion score was calculated: definite invasion = one point; probable invasion = two points; undetermined = three points; probable no-invasion = four points; definite non-invasive = five points.

Results

Pattern Reproducibility

In the first ring study, the reproducibility of pattern classification was performed on 115 cases by 26 pathologists. The 115 cases were as follows: acinar ($n=20$), lepidic (formerly BAC, $n=19$), micropapillary ($n=16$), papillary ($n=19$), solid ($n=20$) and difficult cases ($n=21$). In total, the number of scores for the typical patterns combined and for the difficult cases were 2444 and 546, respectively.

The kappa score (mean and s.d.) calculated between all pathologists for the five typical patterns combined was 0.77 ± 0.07. For the difficult cases, mean and s.d. for Kappa was 0.38 ± 0.14. The distribution of kappa scores for all cases is shown in Figure 1.

Dominant scores were calculated as described before. A dominant score close to 1 is perfect agreement, whereas a score close to 0 corresponds to major disagreement. The distribution of the scores for each pattern is shown in Figure 2. Overall, two patterns have reasonable to good concordance: lepidic and solid. The range of dominant scores for acinar, micropapillary and papillary carcinoma varied to a larger extend. The difficult case category had the lowest average score of agreement.

For the typical cases more than one pattern was recorded in 848 of the 2444 (35%) scores, indicating heterogeneity of adenocarcinoma patterns. In 1048 of the 1205 (87%) diagnostic scores with more than one pattern, two patterns were scored. Three or more scores were present in 13% of the cases. Call overlap existed between all patterns, except between solid and lepidic pattern. Patterns of overlap in adenocarcinoma sub-classification are shown in Table 2. Perhaps not surprisingly, the highest overlap was noted between papillary and micropapillary patterns.

The concordance rates among 26 pathologists to recognize 70% of the submitted typical patterns as a single pattern ranged from 12–65%, lowest for micropapillary and highest for solid types (Table 3). However, when the submitted pattern was recognized as the predominant pattern (combining single plus multiple patterns with the submitted pattern being the predominant one), the concordance rates between submitted and dominant patterns reached 62–100% (Table 3); four of the patterns scoring $\geq 92\%$ except micropapillary. In general, the pattern of overlap was similar for both submitted 'typical' and 'difficult' cases. Examples of overlap in pattern diagnoses are shown in Figure 3.

Invasion Reproducibility

In the second ring study with an emphasis on reproducibility of invasion, 28 pathologists scored the 64 cases. For each case, an invasion score was calculated. A score of 1 with standard deviation of 0 indicated that all 28 scores were definite invasion and vice versa a score of 5 for a case showed perfect agreement for non-invasion. In Table 4, the distribution of invasion scores is shown. Complete agreement was present in only 6 out of 64 cases, combining the probable and definite categories. In 37 cases, at least five readings differed from the majority score (presence or absence of invasion).

In 15 cases, the scores were equivocal for invasion and non-invasion: at least 9 scores were for invasion and at least 9 against invasion. It turned out that the same pathologists were systematically scoring invasion and another group of

Table 4 The invasion score (mean ± standard deviation, s.d.) is shown for each case, ranked from high (4.93 non-invasive score) to low (1.0 invasive score)

Case #	*Invasion score*		*Scores per category*					*Total*
	Mean	*s.d.*	*1 Inv*	*2 Pr Inv*	*3 Undet.*	*4 Pr-NonI*	*5 NonInv*	
71	4.93	0.26	0	0	0	2	26	28
73	4.93	0.26	0	0	0	2	26	28
11	4.86	0.76	1	0	0	0	27	28
74	4.86	0.76	1	0	0	0	27	28
39	4.64	1.06	2	0	0	2	24	28
3	4.57	1.17	2	1	0	1	24	28
57	4.43	1.35	3	1	0	1	23	28
31	4.21	1.40	3	2	0	4	19	28
34	4.21	1.40	3	2	0	4	19	28
46	4.18	1.54	4	2	0	1	21	28
24	4.00	1.54	4	2	2	2	18	28
7	3.25	1.69	8	3	0	8	9	28
17	3.00	1.70	10	2	1	8	7	28
28	3.00	1.56	8	4	1	10	5	28
66	3.04	1.79	11	1	1	6	9	28
52	3.18	1.81	9	3	2	2	12	28
51	2.89	1.77	11	3	0	6	8	28
64	3.00	1.72	9	4	2	4	9	28
4	2.89	1.77	10	5	0	4	9	28
36	2.82	1.76	11	4	0	5	8	28
53	2.61	1.73	13	3	0	6	6	28
14	2.54	1.69	13	3	2	4	6	28
35	2.61	1.73	12	5	0	4	7	28
55	2.64	1.83	13	4	0	2	9	28
9	2.46	1.71	14	3	1	4	6	28
19	2.46	1.45	10	7	2	6	3	28
27	2.14	1.60	17	2	1	4	4	28
59	2.25	1.67	15	5	0	2	6	28
61	2.11	1.45	15	5	0	6	2	28
65	1.89	1.40	18	3	1	4	2	28
15	1.86	1.35	18	3	2	3	2	28
38	1.96	1.40	16	5	2	2	3	28
56	1.93	1.51	18	4	0	2	4	28
40	1.86	1.46	18	5	0	1	4	28
10	1.68	1.28	20	3	1	2	2	28
25	1.54	1.20	23	0	1	3	1	28
49	1.75	1.11	17	4	5	1	1	28
63	1.64	1.28	21	2	1	2	2	28
70	1.57	1.14	21	2	2	2	1	28
12	1.50	1.11	22	2	1	2	1	28
32	1.61	0.92	17	7	2	2	0	28
41	1.50	0.96	20	5	0	3	0	28
45	1.46	0.92	21	3	2	2	0	28
48	1.50	1.04	21	3	2	1	1	28
69	1.50	1.26	23	2	0	0	3	28
75	1.50	0.88	20	3	4	1	0	28
8	1.43	0.84	21	3	3	1	0	28
26	1.46	0.84	20	4	3	1	0	28
67	1.50	1.00	20	5	1	1	1	28
5	1.32	0.94	24	2	0	1	1	28
50	1.39	1.07	23	3	0	0	2	28
16	1.32	0.72	22	4	1	1	0	28
18	1.21	0.69	25	1	1	1	0	28
13	1.25	0.80	24	3	0	0	1	28
29	1.36	0.83	21	6	0	0	1	28
37	1.11	0.57	27	0	0	1	0	28
42	1.14	0.59	26	1	0	1	0	28
47	1.14	0.76	27	0	0	0	1	28
30	1.11	0.42	26	1	1	0	0	28
72	1.11	0.42	26	1	1	0	0	28
21	1.04	0.19	27	1	0	0	0	28
44	1.00	0.00	28	0	0	0	0	28
54	1.00	0.00	28	0	0	0	0	28
68	1.11	0.31	25	3	0	0	0	28

1, definite invasion; 2, probable invasion; 3, undetermined; 4, probable no-invasion; 5, definite no-invasion.

pathologists consistently diagnosed no invasion on the same cases.

Examples of definite non-invasion were similar to AIS/lepidic pattern. Examples of tumor cases with equivocal and definite invasion scores are shown in Figure 4. Morphologic features attributable to discrepant interpretation of the pattern and invasion judgments appear to include: (i) the characteristics of background stroma (fibroblastic reaction *versus* dense fibrosis), (ii) occurrence of inflammation, (iii) tumor architecture, (iv) presence of micropapillary component, and (v) detection of mucinous component.

Kappa statistics for easy cases of invasion (mean value ± s.d.) was 0.55 ± 0.06 when relying on five as well as on three categories (ie, putting together probable invasion and invasion, and probable no-invasion and non-invasion). For the difficult invasion cases, the kappa value was 0.08 ± 0.02 when relying on five and 0.15 ± 0.05 on three categories. Splitting the pathologists in two categories based on the 15 cases with equivocal scoring into a group A, which favored invasion ($n = 14$), and group B, which favored no invasion, the kappa scores for groups A and B for the easy cases (3 categories) were 0.61 ± 0.06 and 0.59 ± 0.07. In contrast, the kappa scores for the difficult cases for group A and group B were 0.16 ± 0.09 and 0.27 ± 0.15, respectively. The improvement in kappa scores for pathologists in groups A and B supports a difference in diagnostic interpretation. Comparing the composition of the two groups, there was some segregation of pathologists in relation to different countries (Chi-2, $P = 0.02$).

Discussion

In these image-based ring studies, substantial reproducibility was found for typical patterns of pulmonary adenocarcinoma subtypes. When multiple patterns are present, and for the assessment of invasion in pulmonary adenocarcinoma, the reproducibility level was good (0.77) for cases showing classic architectural patterns and fair for classic invasion (0.55), but low to poor for problematic pattern and invasion cases.

The kappa score for adenocarcinoma subtyping (0.77–0.38) was higher than in a previously reported study using an older classification (0.18).[11] In our study, it was evident that solid and lepidic patterns without collapse were more reliably recognized than others, such as micropapillary *versus* papillary and acinar *versus* papillary *versus* lepidic, in particular in relation to what constituted invasion (wholly lepidic *versus* other). Thus, a second study was undertaken to examine this area more closely, with the kappa value being very similar overall (0.40) to that for submitted problematic cases in the first phase. Although issues in distinguishing micropapillary *versus* papillary patterns are self-evident,

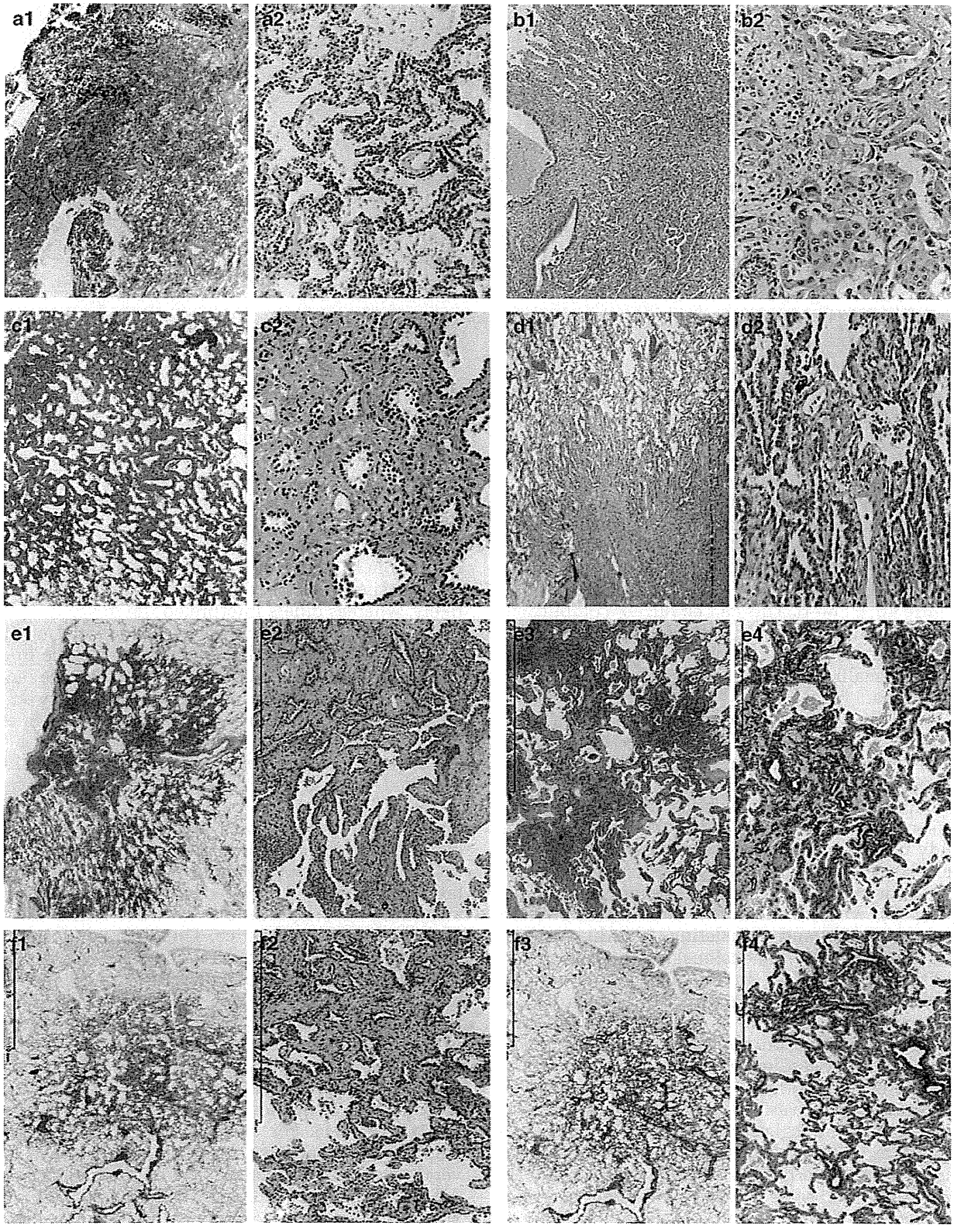

Figure 4 Examples of unanimous absence of invasion (**a**) and definite invasion (**b**) are shown, as well examples of cases (judgement on second image) with split opinion (**c–h**) having at least nine pathologists for invasion ('invasion yes ≥9') and a different group of at least 9 for non-invasion ('NO≥9'). In two cases images of another slide (same case) was available as well (**e3**, **e4** elastic stain and **f3**, **f4** elastic stains).

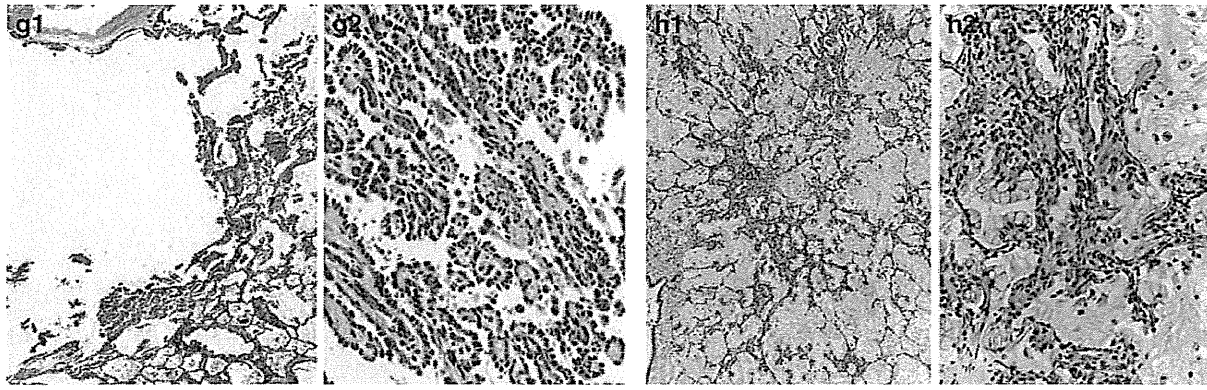

Figure 4 Continued.

problems in distinguishing acinar/papillary patterns from lepidic pattern are not so obvious. However, pulmonary adenocarcinoma poses particular challenges for pathologists through the superimposition of its neoplastic growth on the underlying lung architecture. As they grow into aerated, alveolar tissue, cross-cutting of growth along alveolar walls (lepidic) will mimic papillary structures and desmoplastic reaction will produce acinar structures which in reality are collapsed areas lacking invasion (Figure 4d, g and i). This can be further complicated by pre-existing lung architectural changes such as emphysema or interstitial fibrosis, and inconsistent use of formalin inflation technique to fix the tumor specimens.

Thus, the prime confounder is using a two-dimensional histological section to diagnose a lesion with a complex three-dimensional architecture an issue that not adequately addressed within current definitions, given kappa values in this study. This problem was borne out in both parts of this study in which there were clearly two 'groups', one being very literal (group A) in their application of diagnostic criteria and one being more interpretive (group B), whereas others are more interpretive in their approach and translating 'two-dimensional data' into a 'three-dimensional categorization'. In addition, a difference in the two groups may be related to country of practice. We believe a constructive approach is to improve definitions and increase education on the usage of this terminology.[12,13] Further studies are ongoing in this respect.

Post-study discussion also identified variation in interpretation of various morphological features. First, some pathologists interpreted a stromal component as tumor-related stroma with fibroblasts (also called desmoplastic stroma), whereas others considered the same feature as benign scarring/fibroelastosis (Figure 4c and i). Second, the presence of elastin was variably weighed as representing native alveolar wall by some pathologists but not by others (Figure 4e and f). Third, inflammation in alveolar walls implied invasive disease to some. Fourth, although there was good agreement between pathologists in cases with a prominent micropapillary component, there was variation in interpretation between what some interpreted as focal micropapillary component and tangential cutting of both lepidic and true papillary structures. Finally, some pathologists interpreted a mucinous lepidic component as being invasive, based upon the reasonable assumption that elsewhere in the tumor an invasive component with scarring is highly likely, whereas others interpreted the image in itself as non-invasive (Figure 4h). It is therefore notable that much of the interobserver variation stems from interpretation based on operator experience and opinion, and improved definitions and better education on their usage are required to reduce interobserver variability.

The main limitation of the study was using digitized photographic image to present relevant images of pulmonary adenocarcinoma. The advantages of this approach were that there was precision of diagnosis on specific areas and the study was undertaken in timely manner. The main disadvantage was that the whole section was not examined and therefore the procedure was not representative of daily diagnostic practice. Therefore, to add some context, a low power image was added to the case. Although this did not compensate fully for using a microscope-based approach on whole sections, we believe that this did allow appropriate examination of a pathologist's ability to identify histological patterns in a robust manner. Another limitation is that the review of highly selected images does not represent the frequency of problems encountered in routine practice. For example, in this study great emphasis was placed on distinguishing invasive *versus* non-invasive patterns, when the frequency of AIS, MIA and lepidic predominant patterns occur in 10–20% of all early-stage resected lung adenocarcinomas there is no prognostic difference between the AIS and MIA categories both of which should have 100% 5-year disease-free survival, if completely resected.[3,4]

In conclusion, given that most cases of pulmonary adenocarcinoma show mixed morphology in relation to the five major histological patterns, this study provides strong evidence that a predominant pattern can be reproducibly identified with high concordance among pathologists in resection specimens, thus supportive of the adoption of 'predominant pattern' for subtyping invasive adenocarcinoma in the updated classification, as more data are published highlighting the clinical relevance of this approach. Recognition of the adenocarcinoma *in-situ* pattern is more problematic though kappa values are fair, but this area could be improved by having more precise definitions and subsequent better education on interpretation of existing terminology, and/or additional markers of invasion.

Disclosure/conflict of interest

The authors declare no conflict of interest.

References

1 Travis WD, Brambilla E, Muller-Hermelink KM. Pathology and Genetics: Tumours of the Lung, Pleura, Thymus and Heart. IARC: Lyon, 2004.
2 Travis WD, Brambilla E, Noguchi M, *et al.* International association for the study of lung cancer/american thoracic society/european respiratory society international multidisciplinary classification of lung adenocarcinoma. J Thorac Oncol 2011;6:244–285.
3 Russell PA, Wainer Z, Wright GM, *et al.* Does lung adenocarcinoma subtype predict patient survival?: A clinicopathologic study based on the new International Association for the Study of Lung Cancer/American Thoracic Society/European Respiratory Society international multidisciplinary lung adenocarcinoma classification. J Thorac Oncol 2011;6:1496–1504.
4 Yoshizawa A, Motoi N, Riely GJ, *et al.* Impact of proposed IASLC/ATS/ERS classification of lung adenocarcinoma: prognostic subgroups and implications for further revision of staging based on analysis of 514 stage I cases. Mod Pathol 2011;24:653–664.
5 Campobasso O, Andrion A, Ribotta M, *et al.* The value of the 1981 WHO histological classification in interobserver reproducibility and changing pattern of lung cancer. Int J Cancer 1993;53:205–208.
6 Stang A, Pohlabeln H, Muller KM, *et al.* Diagnostic agreement in the histopathological evaluation of lung cancer tissue in a population-based case-control study. Lung Cancer 2006;52:29–36.
7 Dale I, Lexow P, Skjorten F, *et al.* Reproducibility of tumour typing of lung carcinomas performed according to WHO's recommendation. APMIS 1989;97:351–356.
8 Yesner R. Large cell carcinoma of the lung. Semin Diagn Pathol 1985;2:255–269.
9 Roggli VL, Vollmer RT, Greenberg SD, *et al.* Lung cancer heterogeneity: a blinded and randomized study of 100 consecutive cases. Hum Pathol 1985;16:569–579.
10 Feinstein AR, Wells CK. Lung cancer staging. A critical evaluation. Clin Chest Med 1982;3:291–305.
11 Sorensen JB, Hirsch FR, Gazdar A, *et al.* Interobserver variability in histopathologic subtyping and grading of pulmonary adenocarcinoma. Cancer 1993; 71:2971–2976.
12 Noguchi M, Minami Y, Iijima T, *et al.* Reproducibility of the diagnosis of small adenocarcinoma of the lung and usefulness of an educational program for the diagnostic criteria. Pathol Int 2005;55:8–13.
13 Thunnissen FB, Kerr KM, Brambilla E, *et al.* EU-USA pathology panel for uniform diagnosis in randomised controlled trials for HRCT screening in lung cancer. Eur Respir J 2006;28:1186–1189.

LETTER

doi:10.1038/nature11316

HDAC8 mutations in Cornelia de Lange syndrome affect the cohesin acetylation cycle

Matthew A. Deardorff[1,2]*, Masashige Bando[3]*, Ryuichiro Nakato[3]*, Erwan Watrin[4]*, Takehiko Itoh[5], Masashi Minamino[3], Katsuya Saitoh[3], Makiko Komata[3], Yuki Katou[3], Dinah Clark[1], Kathryn E. Cole[6], Elfride De Baere[7], Christophe Decroos[6], Nataliya Di Donato[8], Sarah Ernst[1], Lauren J. Francey[1], Yolanda Gyftodimou[9], Kyotaro Hirashima[10], Melanie Hullings[1], Yuuichi Ishikawa[11], Christian Jaulin[4], Maninder Kaur[1], Tohru Kiyono[12], Patrick M. Lombardi[6], Laura Magnaghi-Jaulin[4], Geert R. Mortier[13], Naohito Nozaki[14], Michael B. Petersen[9,15], Hiroyuki Seimiya[10], Victoria M. Siu[16], Yutaka Suzuki[17], Kentaro Takagaki[18], Jonathan J. Wilde[1], Patrick J. Willems[19], Claude Prigent[4], Gabriele Gillessen-Kaesbach[20], David W. Christianson[6], Frank J. Kaiser[20], Laird G. Jackson[1,21], Toru Hirota[17], Ian D. Krantz[1,2] & Katsuhiko Shirahige[3,22]

Cornelia de Lange syndrome (CdLS) is a dominantly inherited congenital malformation disorder, caused by mutations in the cohesin-loading protein NIPBL[1,2] for nearly 60% of individuals with classical CdLS[3–5], and by mutations in the core cohesin components SMC1A (~5%) and SMC3 (<1%) for a smaller fraction of probands[6,7]. In humans, the multisubunit complex cohesin is made up of SMC1, SMC3, RAD21 and a STAG protein. These form a ring structure that is proposed to encircle sister chromatids to mediate sister chromatid cohesion[8] and also has key roles in gene regulation[9]. SMC3 is acetylated during S-phase to establish cohesiveness of chromatin-loaded cohesin[10–13], and in yeast, the class I histone deacetylase Hos1 deacetylates SMC3 during anaphase[14–16]. Here we identify HDAC8 as the vertebrate SMC3 deacetylase, as well as loss-of-function *HDAC8* mutations in six CdLS probands. Loss of HDAC8 activity results in increased SMC3 acetylation and inefficient dissolution of the 'used' cohesin complex released from chromatin in both prophase and anaphase. SMC3 with retained acetylation is loaded onto chromatin, and chromatin immunoprecipitation sequencing analysis demonstrates decreased occupancy of cohesin localization sites that results in a consistent pattern of altered transcription seen in CdLS cell lines with either *NIPBL* or *HDAC8* mutations.

Human SMC3 is acetylated by ESCO1 and ESCO2, homologues of yeast Eco1, and has been shown to be important for the establishment of sister chromatid cohesion[10,11,13,17,18]. Using a monoclonal antibody specific for acetylated SMC3 (SMC3-ac)[18], we found that whereas total SMC3 levels remain stable throughout the cell cycle, SMC3-ac rapidly disappears during mitosis, suggesting coordinated deacetylation (Supplementary Fig. 1).

We therefore used RNA interference (RNAi)-based screening of all known human histone deacetylases (HDACs) and sirtuins to identify HDAC8 as the vertebrate SMC3 deacetylase (Supplementary Fig. 2). Loss of HDAC8 activity using either *HDAC8* RNAi or the HDAC8-specific inhibitor PCI-34051 (PCI; Fig. 1a, b) does not alter cell cycle progression, but clearly increases SMC3-ac in both soluble and chromatin fractions throughout the cell cycle (Fig. 1c, lanes 4 and 6, Fig. 1e, lanes 18–22 and 29–33, and Supplementary Fig. 3d, lanes 22–28 and 36–42). Nearly all HDAC8 is present in the soluble fraction in both asynchronous and synchronized cultures (Fig. 1c, e). These data indicate that HDAC8 is present and active throughout the cell cycle, and that soluble SMC3-ac is its deacetylation target, similar to Hos1 in yeast[14–16]. Notably, the increase of SMC3-ac in the soluble fraction in the absence of HDAC8 activity suggests that SMC3-ac dissociates from chromatin but fails to be deacetylated. In addition, we unexpectedly observed few sister chromatid cohesion defects with loss of HDAC8 activity alone (Supplementary Fig. 4).

To understand the role of HDAC8 in genome-wide regulation of cohesin dynamics, we performed chromatin immunoprecipitation sequencing (ChIP-Seq) analysis of synchronized HeLa cells transfected with control or *HDAC8* RNAi (Fig. 2) and immunoprecipitated with either an anti-RAD21 antibody to detect total cohesin or an anti-SMC3-ac antibody. Although total cellular cohesin shows no decrease (Supplementary Fig. 5a, b), and there is a high degree of overlap between SMC3-ac, cohesin and CTCF[19] localization sites in treated and untreated cells, high read numbers and tight correlations between experimental replicates enabled us to identify a 17% loss of total cohesin localization peaks with reduced HDAC8 activity (Fig. 2a–c and Supplementary Fig. 5d–h). Furthermore, despite using conditions that increase total SMC3-ac more than twofold (Fig. 1e and Supplementary Fig. 3d), we note a 16% loss of SMC3-ac localization sites with HDAC8 reduction (Fig. 2a–d and Supplementary Fig. 5f, g). Finally, we found that in both control and HDAC8-depleted cells, SMC3-ac preferentially localizes to downstream regions of genes relative to the distribution of RAD21 (Fig. 2c, d and Supplementary Fig. 5f, g). Together, this data demonstrates decreased occupancy of cohesin localization sites with the loss of HDAC8 activity, an observation similarly noted for *NIPBL* haploinsufficient CdLS cells[20].

With the known role of cohesin regulation in CdLS and the observations that a reduction in either HDAC8 or NIPBL leads to decreased cohesin occupancy of localization sites, we proposed that *HDAC8* mutations may cause CdLS. We screened this X-linked gene in 154 individuals with CdLS negative for mutations in *NIPBL*, *SMC1A* and

[1]Division of Human Genetics and Molecular Biology, The Children's Hospital of Philadelphia, Pennsylvania 19104, USA. [2]The Department of Pediatrics, University of Pennsylvania Perelman School of Medicine, Philadelphia, Pennsylvania 19104, USA. [3]Research Center for Epigenetic Disease, Institute for Molecular and Cellular Biosciences, The University of Tokyo, Tokyo 113-0032, Japan. [4]Centre National de la Recherche Scientifique (CNRS), Research Institute of Genetics and Development (IGDR), Faculté de Médecine, Rennes 35043, France. [5]School and Graduate School of Bioscience and Biotechnology, Tokyo Institute of Technology, Yokohama 226-8503, Japan. [6]Department of Chemistry, University of Pennsylvania, Philadelphia, Pennsylvania 19104, USA. [7]Center for Medical Genetics, Ghent University Hospital, 9000 Ghent, Belgium. [8]Institut für Klinische Genetik, Technische Universität Dresden, 01307 Dresden, Germany. [9]Department of Genetics, Institute of Child Health, 11527 Athens, Greece. [10]Division of Molecular Biotherapy, Japanese Foundation for Cancer Research, Tokyo 135-8550, Japan. [11]Department of Pathology, Japanese Foundation for Cancer Research, Tokyo 135-8550, Japan. [12]Virology Division, National Cancer Center Research Institute, Tokyo 104-0045, Japan. [13]Department of Medical Genetics, Antwerp University Hospital and University of Antwerp, B-2650 Antwerp, Belgium. [14]Bio-Frontier Research Center, Tokyo Institute of Technology, Yokohama 226-8503, Japan. [15]Department of Clinical Genetics, Aalborg Hospital, Aarhus University Hospital, 9100 Aalborg, Denmark. [16]Medical Genetics, University of Western Ontario, London, Ontario N6A 5W9, Canada. [17]Graduate School of Frontier Sciences, The University of Tokyo, Tokyo 277-8561, Japan. [18]Experimental Pathology, Japanese Foundation for Cancer Research, Tokyo 135-8550, Japan. [19]GENDIA, 2020 Antwerp, Belgium. [20]Institut für Humangenetik Lübeck, Universität zu Lübeck, 23538 Lübeck, Germany. [21]Department of Obstetrics and Gynecology, Drexel University School of Medicine, Philadelphia, Pennsylvania 19102, USA. [22]CREST, JST, K's Gobancho, 7, Gobancho, Chiyoda-ku, Tokyo 102-0076, Japan.
*These authors contributed equally to this work.

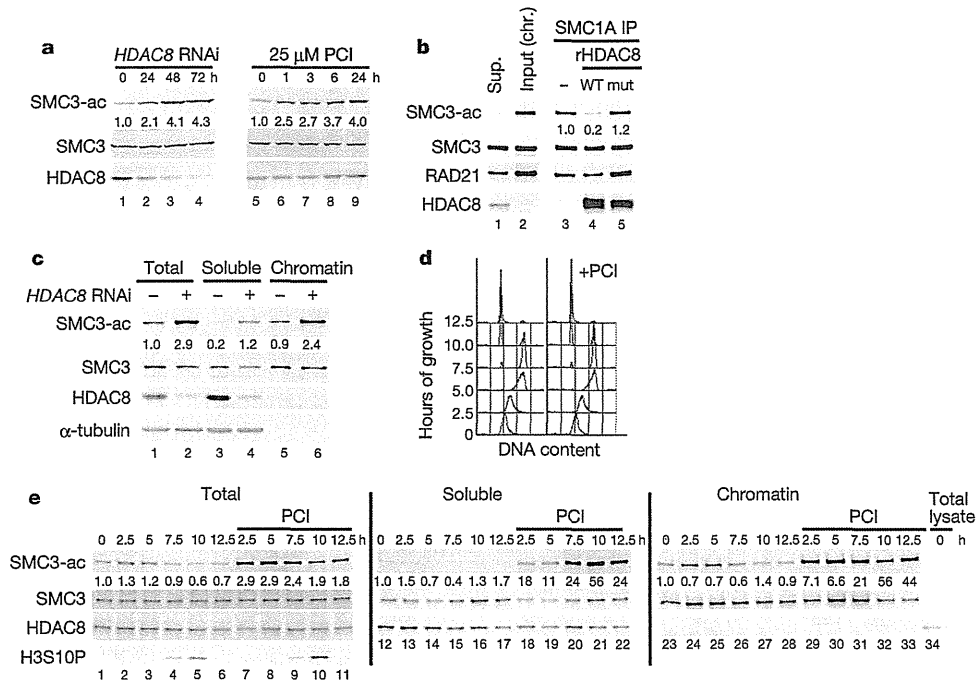

Figure 1 | HDAC8 is an SMC3 deacetylase. a, HeLa cells were transfected with *HDAC8* short interfering RNA (siRNA; lanes 1–4) or incubated with 25 μM PCI, the HDAC8-specific inhibitor (lanes 5–9), for the indicated times. Total cell lysates were prepared and analysed by immunoblotting using anti-SMC3-ac, SMC3 and HDAC8 antibodies. Numbers beneath SMC3-ac bands indicate quantification of SMC3-ac levels normalized to SMC3 levels and the 0 h time point. **b**, Acetylated SMC3 was prepared by co-immunoprecipitation with SMC1A from HeLa cell chromatin extracts. Immunoprecipitates (IP) were incubated with recombinant purified HDAC8 (rHDAC8) or mutant (mut) HDAC8 protein at 30 °C for 1 h and analysed by immunoblotting as in **a**. Chr., chromatin; Sup., supernatant; WT, wild type. **c**, Unsynchronized HeLa cells transfected with *HDAC8* siRNA for 48 h were fractionated into soluble and chromatin fractions and immunoblotted as in **a**. **d**, HeLa cells were synchronized by double thymidine arrest, and released in the presence or absence of 25 μM PCI for the indicated time and verified by FACS analysis for cell cycle progression. **e**, Cell extracts of the PCI-treated cells in **d** were fractionated into soluble and chromatin fractions and analysed by immunoblotting as in **a**. Histone H3 Ser 10 phosphorylation (H3S10P) is a marker of prophase and the onset of mitosis.

SMC3, as well as *RAD21* (also known as *SSC1*), *STAG2*, *ESCO1*, *ESCO2* and *MAU2* (also known as *SCC4*). We identified four *de novo* missense mutations and one *de novo* nonsense mutation in *HDAC8* (Supplementary Table 1 and Fig. 3a). In addition, one familial mutation (c.1001A>G; p.H334R) was identified in a boy, his mildly affected sister and his unaffected mother, in which the mutant allele was inactivated in her blood. This mutation was also one of the *de novo* mutations in an unrelated girl. None of the mutations was seen in 290 ethnically matched control chromosomes or in 629 individuals of the 1000 Genomes Project[21]. Despite the small numbers and the varied clinical features in females due to random X-chromosome inactivation, these children demonstrate growth, cognitive and facial features consistent with those caused by mutations in *NIPBL* ('classical' CdLS). Both expression studies (Supplementary Fig. 6a) and X-chromosome inactivation studies (data not shown) demonstrate complete skewing towards the normal allele in the blood of females with *HDAC8* mutations, indicating strong selection against the mutation. This limited the number of cell lines available for subsequent studies. However, immunoblotting demonstrated minimal HDAC8 protein expression in lymphoblastoid cell lines (LCLs) from a hemizygous boy with a p.G320R mutation as well as the skin fibroblasts from a female lyonized to express a p.H180R mutant allele (Fig. 3b), indicating protein instability in each case. Consistent with this, assessment of SMC3-ac demonstrates increased levels in both the p.G320R LCLs and the p.H180R fibroblasts, whereas the total amount of SMC3 (Fig. 3b) and cell cycle distribution for the LCLs are unchanged (Supplementary Fig. 6b).

We expressed the HDAC8 missense mutations in *Escherichia coli*, purified and assayed each for deacetylase activity. These data (Fig. 3c) demonstrate that the p.H180R mutation severely abrogates HDAC8 deacetylase activity, and demonstrate significant activity losses for the p.G320R, p.T311M and p.H334R mutations, consistent with high conservation of each residue and position in the structure of HDAC8–substrate complexes[22,23] (Fig. 3d and Supplementary Fig. 6c–e). Finally, purified wild-type, but not mutant HDAC8, can rescue the SMC3 overacetylation seen in *HDAC8* mutant LCLs (Supplementary Fig. 6g, h).

We have previously demonstrated that mutations in *NIPBL*, the primary cause of CdLS, result in consistent, reproducible changes of genes expressed from LCLs derived from individuals with CdLS[20]. Using Nanostring multiplex expression analysis to avoid variation introduced by PCR or RNA amplification-based assessments and a previously validated 32-gene CdLS classifier set[20], we compared the expression of LCLs from the male with the p.G320R mutation and from two girls (with the p.H180R and p.H334R mutations) who express only the normal allele in these cells, to 10 normal controls and 12 LCLs with loss of function *NIPBL* mutations. In this assay, the aggregate 32-gene LCL expression profile of the single male with an *HDAC8* mutation strongly correlates with that seen in *NIPBL*-mutant cell lines, whereas the profile for the two female lines, which express the wild-type allele, correlates with normal controls (Fig. 3e). These data support the hypothesis that loss of HDAC8 activity results in widespread transcriptional dysregulation as seen in *NIPBL*-mutated CdLS cells. The loss of cohesin-binding sites in *HDAC8* RNAi-depleted HeLa cells and in *NIPBL*-mutant LCLs[20] was also noted in the p.G320R HDAC8-mutant LCLs and fibroblasts derived from the girl with the p.H180R mutation, in which small but consistent changes in transcriptional dysregulation were also noted (Supplementary Figs 6a, 7 and 8). Together, these data suggest that loss of HDAC8 activity leads to a common pathogenic mechanism for classical CdLS that converges on the reduction of bound cohesin complexes.